

Search for chameleons with CAST

V. Anastassopoulos^a, M. Arik^{b,1}, S. Aune^c, K. Barth^d, A. Belov^e, H. Bräuninger^f, G. Cantatore^g, J. M. Carmona^h, S. A. Cetin^b, F. Christensenⁱ, J. I. Collar^j, T. Dafni^h, M. Davenport^{d,*}, K. Desch^k, A. Dermenev^e, C. Eleftheriadis^l, G. Fanourakis^m, E. Ferrer-Ribas^c, P. Friedrich^f, J. Galán^c, J. A. García^h, A. Gardikiotis^a, J. G. Garza^h, E. N. Gazisⁿ, T. Geralis^m, I. Giomataris^c, C. Hailey^o, F. Haug^d, M. D. Hasinoff^p, D. H. H. Hoffmann^q, F. J. Iguez^h, I. G. Irastorza^h, J. Jacoby^r, A. Jakobsenⁱ, K. Jakovčić^s, J. Kaminski^k, M. Karuza^{t,g}, M. Kavuk^{b,2}, M. Krčmar^s, C. Krieger^k, A. Krüger^{d,3}, B. Lakić^s, J. M. Laurent^d, A. Liolios^l, A. Ljubičić^s, G. Luzón^h, S. Neff^q, I. Ortega^{h,d}, T. Papaevangelou^c, M. J. Pivovarov^u, G. Raffelt^v, H. Riege^q, M. Rosu^d, J. Ruz^u, I. Savvidis^l, S. K. Solanki^{w,4}, T. Vafeiadis^{d,l,*}, J. A. Villar^h, J. K. Vogel^u, S. C. Yildiz^{b,5}, K. Zioutas^{d,a}, (CAST Collaboration), and P. Brax⁶, I. Lavrentyev⁷, A. Upadhye⁸

^aPhysics Department, University of Patras, Patras, Greece

^bDogus University, Istanbul, Turkey

^cIRFU, Centre d Etudes Nucléaires de Saclay (CEA-Saclay), Gif-sur-Yvette, France

^dEuropean Organization for Nuclear Research (CERN), Genève, Switzerland

^eInstitute for Nuclear Research (INR), Russian Academy of Sciences, Moscow, Russia

^fMax-Planck-Institut für Extraterrestrische Physik, Garching, Germany

^gIstituto Nazionale di Fisica Nucleare (INFN), Sezione di Trieste and Università di Trieste, Trieste, Italy

^hInstituto de Física Nuclear y Altas Energías, Universidad de Zaragoza, Zaragoza, Spain

ⁱDanish Technical University-Space (DTU), Copenhagen, Denmark

^jEnrico Fermi Institute and KICP, University of Chicago, Chicago, IL, USA

^kPhysikalisches Institut, Universität of Bonn, 53115 Bonn, Germany

^lAristotle University of Thessaloniki, Thessaloniki, Greece

^mNational Center for Scientific Research "Demokritos", Athens, Greece

ⁿNational Technical University of Athens, Athens, Greece

^oColumbia University (CU), New York, United States of America

^pDepartment of Physics and Astronomy, University of British Columbia, Vancouver, Canada

^qTechnische Universität Darmstadt, IKP, Darmstadt, Germany

^rJ. W. Goethe-Universität, Institut für Angewandte Physik, Frankfurt am Main, Germany

^sRudjer Bošković Institute, Zagreb, Croatia

^tPhysics Department and Center for Micro and Nano Sciences and Technologies, University of Rijeka, Croatia

^uLawrence Livermore National Laboratory, Livermore, CA 94550, USA

^vMax-Planck-Institut für Physik (Werner-Heisenberg-Institut), München, Germany

^wMax-Planck-Institut für Sonnensystemforschung, Göttingen, Germany

Abstract

In this work we present a search for (solar) chameleons with the CERN Axion Solar Telescope (CAST). This novel experimental technique, in the field of dark energy research, exploits both the chameleon coupling to matter (β_m) and to photons (β_γ) via the Primakoff effect. By reducing the X-ray detection energy threshold used for axions from 1 keV to 400 eV CAST became sensitive to the converted solar chameleon spectrum which peaks around 600 eV. Even though we have not observed any excess above background, we can provide a 95% C.L. limit for the coupling strength of chameleons to photons of $\beta_\gamma \lesssim 10^{11}$ for $1 < \beta_m < 10^6$.

Keywords: chameleon, CAST, SDD, X-ray, tachocline, dark energy

2015 MSC: 00-01, 99-00

*Corresponding author.

Email addresses: Martyn.Davenport@cern.ch (M. Davenport),

Theodoros.Vafeiadis@cern.ch (T. Vafeiadis)

¹Pr. addr.: Bogazici University, Istanbul, Turkey.

²Pr. addr.: Bogazici University, Istanbul, Turkey.

³Pr. addr.: Hochschule Karlsruhe Technik und Wirtschaft, Univ. of Applied Sciences, Moltkestr. 30, 76133 Karlsruhe, Germany.

⁴Sec. affiliation: School of Space Research, Kyung Hee University, Yongin, Republic of Korea.

⁵Pr. addr.: Dep. of Physics and Astronomy, University of California Irvine, Irvine, CA 92697, USA.

⁶Affiliation: Institut de Physique Théorique, CEA, IPHT, CNRS, URA 2306, F-91191 Gif/Yvette Cedex, France.

⁷Affiliation: Boston University, Boston, MA 02215, USA.

1. Introduction

The dark sector of cosmology represents a big challenge in fundamental physics. In particular, dark energy [1, 2], which is responsible for the accelerated expansion of the Universe, could be due to the existence of a scalar field like the postulated chameleon [3, 4, 5] (for a comprehensive theoretical treatment we refer to [6]). Although a high energy description of chameleons derived from an ultraviolet completion such as

⁸Affiliation: Physics Dep., University of Wisconsin-Madison, 1150 University Avenue, Madison, WI 53706, USA.

string theory is still missing, this type of low energy model is suggestive enough to justify novel investigations like the one presented in this work.

Chameleons can be created in the solar tachocline [7, 8], a region inside the Sun at a distance of around $0.7 R_{\odot}$ from the centre, where intense magnetic fields are widely believed to be present. They have non-linear self-interactions and interactions with matter which give them an “effective mass” dependent on the ambient mass (energy) density. They would have a very small effective mass in outer space or in the evacuated magnet cold bores of CAST [9] but a large effective mass inside the detector material of most terrestrial dark matter experiments. Their corresponding energies generally exceed the chameleon effective mass inside matter and thus they traverse materials with hardly any interaction, making detection difficult.

One uncertainty in chameleon searches is the possibility of “fragmentation”, by which chameleon particles self-interact to generate a larger number of lower-energy chameleons. If fragmentation within the Sun were frequent, then solar chameleons would have energies close to their masses. The treatment of chameleon fragmentation as a coherent, semiclassical process in [10] is inapplicable to the Sun, and a proper calculation may require a UV completion to low-energy chameleon models. Since fragmentation cannot reliably be computed in the Sun, we do not consider it here further.

To investigate the existence of exotica like chameleons we present the first results with a new experimental technique [7], by transforming an axion helioscope to a chameleonic one. Chameleons, like axions, can be created and detected by the Primakoff effect inside a transverse magnetic field, with their conversion efficiency being optimised in vacuum. In addition, the spectral shape of solar chameleons peaks at about 600 eV, and it is interesting to notice that below ~ 1 keV the conversion probability from chameleon-to-photon via the Primakoff effect is quasi-constant [8].

In this paper we discuss the upper limit on the chameleon to photon coupling strength (β_{γ}) for a wide range of their coupling to matter. Our result on β_{γ} is comparable with the one obtained by the GammeV-CHASE (hereafter CHASE) experiments in a laser cavity [11, 12]. We explore uncertainties in the tachocline magnetic field, the precise radius and width of this region and the fraction of solar luminosity emitted as chameleons. We also consider higher powers of the chameleon potential and show that our limit, $\beta_{\gamma} \lesssim 10^{11}$, stands almost independent of the type of inverse power law potential used.

2. The experiment

The detection of solar chameleons can be performed with an axion helioscope like CAST via the inverse Primakoff effect. The relevant chameleon-to-photon coupling strength (β_{γ}) replaces the axion-to-photon coupling constant ($g_{a\gamma}$). In the tachocline where the density is relatively low and strong magnetic fields are present, chameleons can be produced by the Primakoff effect. Their expected spectrum originates from the

photon thermal spectrum and is modified by the creation probability in such an environment which is proportional to the square of the photon energy (ω^2) times a factor of $\omega^{-1/2}$ which derives from the fact that the photons perform a random walk in the Sun. All in all, this shifts the peak of the spectrum of produced chameleons from the photon temperature in the tachocline at around 200 eV to a much larger value of 600 eV. Note that this is a lower value than the one for the axions from the solar core, which are expected to appear with energies in the multiple keV range. To study solar chameleons in CAST the cold bores should be in vacuum, whilst the detector should ideally be sensitive to the 150 – 1500 eV energy range.

After running with vacuum in the magnet bores in 2003 and 2004 [13, 14], and with helium-filled cold bores between 2005 and 2012 [15, 16, 17], CAST was configured once again for vacuum running in 2013 by removing the thin X-ray windows (which had a cutoff at 1 keV). This produced an uninterrupted vacuum line, running from the vacuum port of the magnet cryostat at one end of the magnet, through the cold bores of the 10 m prototype LHC magnet, to the exit port of the cryostat on the opposite side of the magnet.

X-ray detectors on CAST in the period from 2003 to 2012 have operated with energy thresholds above 1 keV to cover the solar axion energy spectrum. The 2013 vacuum setup allowed sub-keV photons to exit the magnet cold bore and reach the X-ray detectors without absorption. Sub-keV sensitive detectors were then able to explore this energy range.

The experiment described here took place in a short running period before the installation of a powerful combination of the existing X-ray telescope (MPE-AbriXas flight spare) and a newly developed InGrid detector [18], capable of simultaneous sub-keV and multi-keV operation. A sub-keV detector system was assembled using mostly commercially available equipment to exploit this first period of vacuum running. The detector was installed on the sunrise side of the experiment taking data during the morning solar tracking of the magnet for ~ 90 min each day. The magnetic field length was 9.26 m, the cold bore diameter 43 mm and the field 9 T.

3. The detector system

The X-ray detector system comprised a Silicon Drift Detector (SDD) [19] and a preamplifier-readout card⁹ inside a vacuum enclosure. The 1.1 W dissipated from the preamplifier was removed by a copper heat exchanger block. The SDD signal was routed to a Digital Pulse Processor (DPP)¹⁰. The DPP was operated with a peaking time of 5.6 μ s in gated mode using the gate provided by the preamplifier-readout card. The energy threshold of the device was set to 167 eV.

The detector chosen was a single channel, non-imaging SDD, without a vacuum window, in this case a commercial research

⁹Readout Electronics Board (pulsed reset) from PNDetector, Munich, Germany.

¹⁰PX5-Digital Pulse Processor AMPTEK, Bedford, USA.

grade device¹¹, with a large surface of 89 mm² effectively covering 6.13% of the magnet cold bore (diameter 43 mm). The device was made from 450 μ m thick polysilicon technology with an entrance window optimized for light elements. The energy resolution of the device is 39 eV FWHM at 277 eV. Due to the sharply rising noise profile at low energies, the threshold used in the analysis was set at 400 eV. The typical quantum response is shown in Fig. 1; the quantum efficiency (ϵ_q) exceeds 80% for photon energies above 400 eV. The background level for the device was $\sim 10^{-3}$ cts/keV/cm²/s in the range 400 – 1500 eV and was independent of the detector temperature over the range -25° to -45° C. The SDD was operated at -30° C using an integrated double peltier cooling element; the 1.0 W from the SDD was also removed by the copper heat exchanger. The detector temperature remained constant when tilting the magnet during solar tracking.

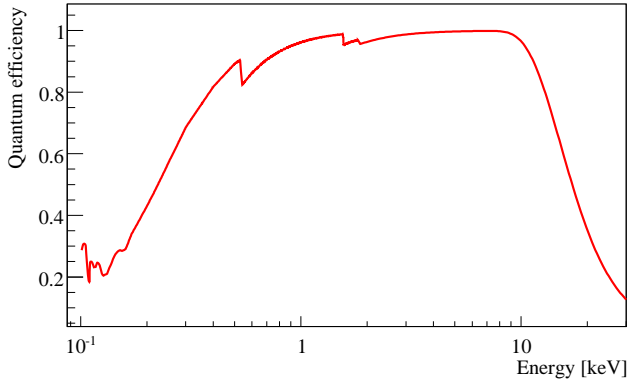


Figure 1: Quantum efficiency of the SDD.

The detector system inside the vacuum vessel was connected directly to the cold bore vacuum port gate valve (on the left in Fig. 2). The vacuum vessel was made from an iso-K DN 100 stainless steel tube connected to a custom-built copper end flange.

Shielding inside the vacuum vessel was provided by the OFE copper back flange plus an OFE copper inner cylinder and upstream collimator; the vacuum vessel was surrounded by 6 cm thick lead rings, and lead plates with thickness between 1 and 3 cm. The turbo-pumped dry vacuum system operated at a pressure of 1.2×10^{-6} mbar with the cryostat gate valve opened for data taking.

4. Laboratory tests

Prior to installation on CAST, the SDD was tested in a laboratory at CERN on a variable energy X-ray vacuum beam line [20]. The system provided calibration energies between 0.28 and 10 keV. Using the characteristic emission lines with the best statistics, the energy resolution (FWHM) of the detector was defined for various energies. In Fig. 3 the measured FWHM versus the energy is shown.

¹¹SDD-100-130pnW-OM-ic Premium Line from PNDetector, Munich, Germany.

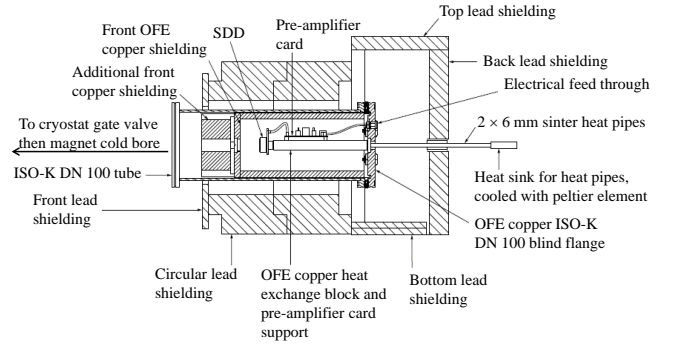


Figure 2: SDD detector vacuum and shielding system.

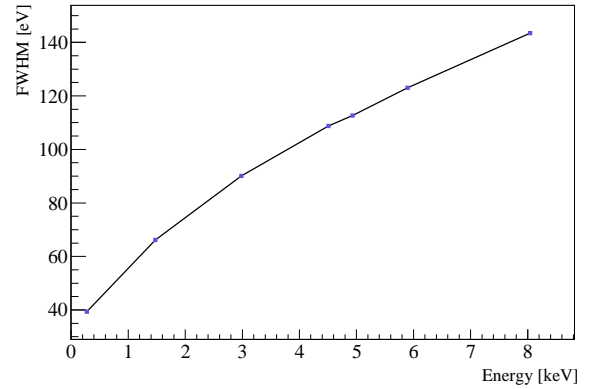


Figure 3: Measured FWHM of the SDD versus energy.

During the first run of the detector on the X-ray beam line, a noticeable drop in the count rate with time was observed in the energy range 300 – 800 eV with the detector operated at -46° C and in a relatively poor vacuum of 4×10^{-5} mbar. Substances outgassing from the electronics components and then being cryo-pumped on to the cold entrance window surface caused a loss of efficiency.

In order to quantify this phenomenon, further measurements were taken at the nominal detector operating temperature of -30° C, using the bremsstrahlung spectrum of the Ag target in the X-ray generator. After a few hours at room temperature, the detector was cooled to -30° C at a vacuum pressure of 2.5×10^{-6} mbar. Then several 5 min measurements of the same spectrum were taken over the course of the next 25 h to determine the loss of efficiency with time. Returning the detector to room temperature for 1 h was enough to fully recover its efficiency.

Monte-Carlo simulations verified that the loss in efficiency of the SDD could be explained by a film deposition with a thickness that increases uniformly with time. Moreover the absorption spectrum of a simple hydrocarbon film (C_3H_6) proved to be sufficient when folded with the resolution of the detector to reproduce the measured absorption. In Fig. 4 the comparison of the spectra taken after 3, 7, 21 and 25 h of operation of the detector, with the initial one (directly after cool down) are displayed, together with the simulated values. A chi-squared fit was performed between the simulated and real data

to determine the evolution of the thickness of the hydrocarbon film. The result is shown in Fig. 5, where the evolution of the transmission of the hydrocarbon film is shown for each bin of 100 eV. These data were used for the parameterization of the transmission of the hydrocarbon film, versus time and energy, in order to calculate the overall efficiency of the detector to photons in the range 400 – 1500 eV. Our correction for this effect to the tracking data is less than 3%. Our SDD proved to be significantly more efficient than an SDD fitted with a vacuum window.

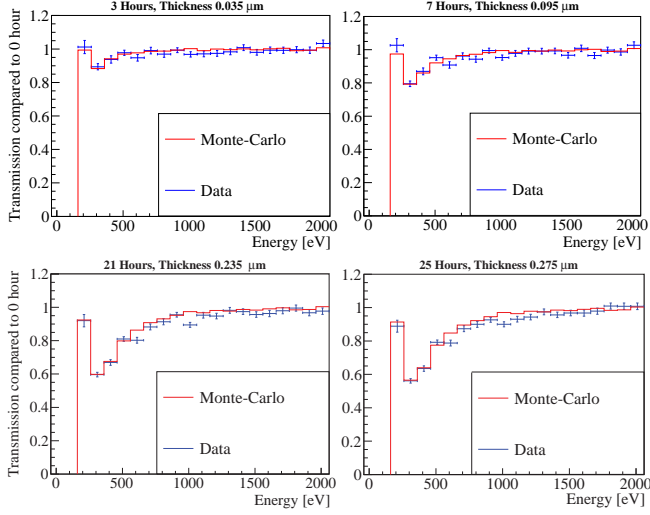


Figure 4: Comparison of the spectrum that was taken immediately after the cool-down of the SDD, with the ones taken 3, 7, 21 and 25 h later. The form of the histograms clearly indicates a progressive deposition of an absorption layer on the detector surface. The simulated data (continuous line) correspond to the deposition of a C_3H_6 film on the surface of the detector.

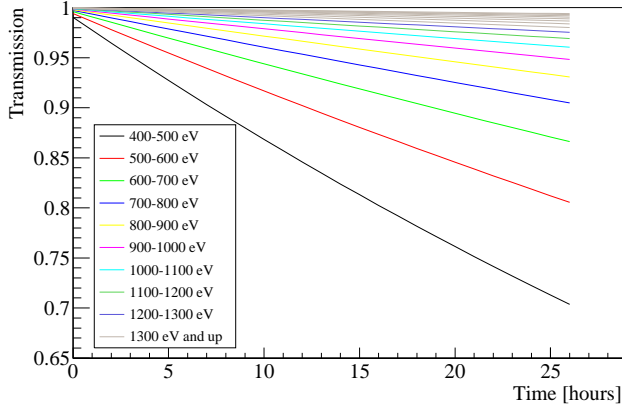


Figure 5: The drop in transmission due to the increasing deposition of the hydrocarbon film on the surface of the detector, for each energy bin, at the energy range of interest (400 – 1500 eV).

5. Data taking

The tests in the laboratory indicated that the detector required 1 h at ambient temperature in order to fully recover its

lost efficiency. To ensure maximum efficiency of the detector during the sunrise solar tracking, the detector was set to ambient temperature 2 h before data taking and set to -30°C only 30 min before the sunrise solar tracking started. At the end of the sunrise solar tracking the detector was again set to ambient temperature and then set back to -30°C about 30 min before the evening solar tracking. The detector then remained at nominal operating temperature until the next day, 2 h before sunrise solar tracking, when the cycle was repeated. The data taking took place over 9 sunrise solar trackings amounting to 15.2 h of exposure. The background data consisted of 13.8 h of sunset solar tracking and 94.2 h of overnight background runs with the magnet stationary (108 h in total).

The operational energy threshold for the SDD was 167 eV which produced an acquisition rate of ~ 5 mHz over the range up to 10 keV. This rate was quasi-constant and independent of the magnet motion. Over the whole data taking period of 9 days the SDD rate between 400 and 1500 eV was 1.40 ± 0.16 mHz (15.2 h sunrise tracking) corresponding to 1.43×10^{-3} cts/keV/cm²/s. The rate obtained during background runs was 1.42 ± 0.06 mHz (108 h). The spectra of the sunrise tracking and background rates are shown in Fig. 6.

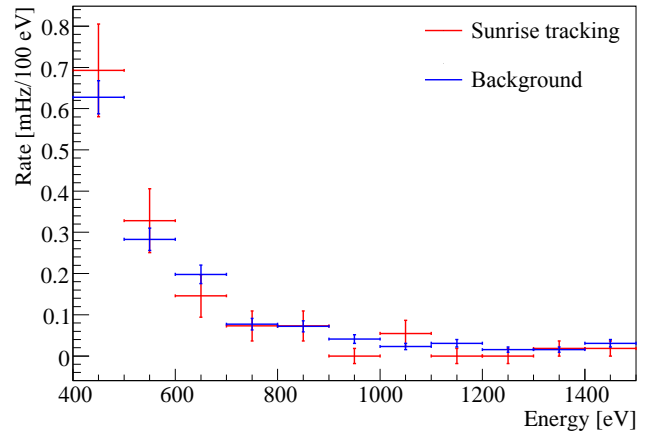


Figure 6: Combined spectra of the rate during sunrise tracking and during background measurements.

The effect of the internal copper and external lead shielding in the background can be gauged by the comparison between data taken in the X-ray laboratory (unshielded) and from CAST (both internal copper and external lead shielding). The background rate in the range 1.5 – 10 keV of the SDD in the X-ray beam line was 3.86 ± 0.34 mHz (compared to 1.42 ± 0.06 mHz on CAST) and for 400 – 1500 eV was 2.31 ± 0.26 mHz (compared to 1.42 ± 0.06 mHz on CAST), indicating the presence of electronic noise at low energies. Analysis of the energy spectra for all background runs taken over typically 13.5 h each day showed no statistically significant decrease with time in the spectra at low energies (300 – 600 eV), as shown in Fig. 7.

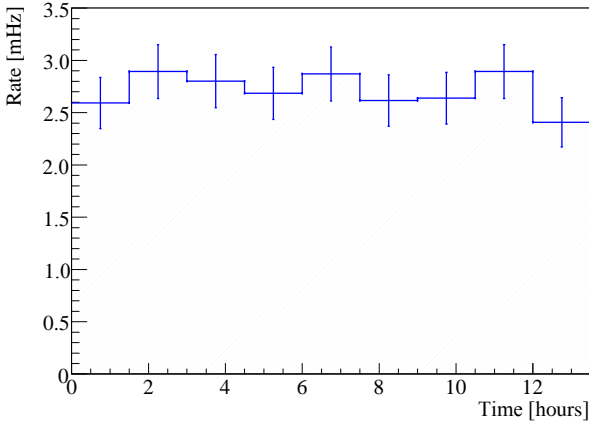


Figure 7: Evolution of low energy background (300 – 600 eV) with time.

6. Theoretical chameleon spectrum

Chameleons can be produced by mixing with the photon flux emanating from the Sun's core [7, 8]. The conversion probability of photons into chameleons in a magnetised region with a constant magnetic field B over a distance l is given by [8]

$$p_{\gamma \rightarrow \phi}(l) = \frac{\beta_\gamma^2 B^2 l_\omega^2}{4m_{\text{Pl}}^2} \sin^2 \frac{l}{l_\omega}, \quad (1)$$

where the Planck mass is $m_{\text{Pl}} \sim 2 \times 10^{18}$ GeV, the coherence length is given by $l_\omega = \frac{4\omega}{m_{\text{eff}}^2}$ and the effective mass of the chameleon is

$$m_{\text{eff}}^2 = \beta_m^{(n+2)/(n+1)} \omega_\rho^2 - \omega_{pl}^2, \quad (2)$$

where we have defined

$$\omega_\rho^2 = \frac{(n+1)\rho}{m_{\text{Pl}}} \left(\frac{\rho}{n m_{\text{Pl}} \Lambda^{n+4}} \right)^{1/(n+1)} \quad (3)$$

and the plasma frequency is $\omega_{pl}^2 = \frac{4\pi\alpha\rho}{m_e m_p}$. We have introduced the fine structure constant $\alpha \sim 1/137$ and the proton and electron masses m_p and m_e . The mass of the chameleon depends on the density ρ and the coupling to matter β_m . The index $n > 0$ defines the chameleon model and comes from the scalar potential $\frac{\Lambda^{n+4}}{\phi^n}$ where $\Lambda \sim 10^{-3}$ eV is the dark energy scale. We have assumed that the mixing angle $\theta = \frac{\omega B \beta_\gamma}{m_{\text{Pl}} m_{\text{eff}}^2} \lesssim 1$.

Photons in the solar plasma perform a random walk. When they have moved by a radial distance $d(l)$ in one second, they have undergone $N(l)$ collisions with the plasma where l is the distance between two collisions

$$N(l) = \frac{c}{d(l)}, \quad d(l) = l \sqrt{N(l)}. \quad (4)$$

The distance l is distributed according to a Poisson law with average λ given by the mean free path. In a solar region of width ΔR where the mean free path and the magnetic field are (nearly) constant, the conversion probability into chameleons is given by

$$d\mathcal{P}(l) = \frac{\Delta R}{d(l)} N(l) p_{\gamma \rightarrow \phi}(l) e^{-l/\lambda} \frac{dl}{\lambda}. \quad (5)$$

Summing over the total number of cells defined by $R_\odot/\Delta R$ we get the conversion rate per unit length

$$\frac{d\mathcal{P}}{dx} = \sqrt{\frac{c}{l_\omega(r)}} \frac{\beta_\gamma^2 B^2(r) l_\omega^2(r) R_\odot}{4m_{\text{Pl}}^2 \lambda(r)} \int_0^\infty \frac{\sin^2 y}{y^{3/2}} e^{-l_\omega(r)y/\lambda(r)} dy, \quad (6)$$

which depends on the radius r from the centre of the Sun. The conversion probability is obtained by integrating the conversion rate over $x = r/R_\odot$.

In the tachocline, and for the range of energies of interest it turns out that $l_\omega(r) \ll \lambda(r)$, implying that the conversion rate simplifies greatly

$$\frac{d\mathcal{P}}{dx} = C \sqrt{\frac{c}{l_\omega(r)}} \frac{\beta_\gamma^2 B^2(r) l_\omega^2(r) R_\odot}{4m_{\text{Pl}}^2 \lambda(r)}, \quad (7)$$

where $C = \int_0^\infty \frac{\sin^2 y}{y^{3/2}} dy$. Notice that the spectrum depends on $\omega^{3/2}$ and not ω^2 due to the random walk of the photons in the solar plasma, and the $\sqrt{N(l)}$ excursions of the photons covering the distance $d(l)$ in one second. In practice and in the absence of a resonance where m_{eff}^2 vanishes somewhere in the tachocline for a large value of β_m , the effective mass of the chameleon is essentially independent of the coupling to matter β_m . This implies that the conversion probability depends only on the coupling to photons, β_γ .

The chameleon flux leaving the Sun is simply given by

$$\Phi_{\text{cham}}(\omega) = \int_0^1 n_\gamma p_\gamma \frac{d\mathcal{P}}{dx} dx, \quad (8)$$

where the integrand vanishes outside the tachocline. It depends on the photon flux n_γ and the photon spectrum p_γ . The spectral dependence of this flux is in $\omega^{3/2} p_\gamma(\omega) \sim \frac{\omega^{7/2}}{e^{\omega/T} - 1}$, where T is the photon temperature in the tachocline, with a maximum around $\omega_{\text{max}} \sim 600$ eV. The total luminosity of the Sun in chameleons is given by

$$L_{\text{cham}} = \int_0^\infty \omega \Phi_{\text{cham}}(\omega) d\omega, \quad (9)$$

which depends on β_γ^2 . We calibrate β_γ in such a way that the chameleon luminosity does not exceed 10% of the solar luminosity. For $n = 1$ and a tachocline of width $0.01 R_\odot$ located at a radius $0.7 R_\odot$ and a magnetic field of 10 T, the chameleons saturate the solar luminosity bound for $\beta_\gamma^{\text{sun}} = 10^{10.81}$. As the number of regenerated photons in the CAST detector goes like β_γ^4 , this gives an upper limit to the number of photons that one may expect to detect. In the following, we shall see how the likelihood analysis takes into account the solar bound on the chameleon luminosity.

7. Analysis and results

The cold bore diameter of 43 mm at the upstream end of the magnetic region of $L_0 = 9.26$ m results in an aperture of 3.5 mrad as seen by the SDD. Chameleons emitted from larger angles up to the tachocline (6.5 mrad for a sphere diameter of $0.7 R_\odot$) traverse less than the full magnetic length of the magnet. A simulation of the CAST geometry was carried out and the results

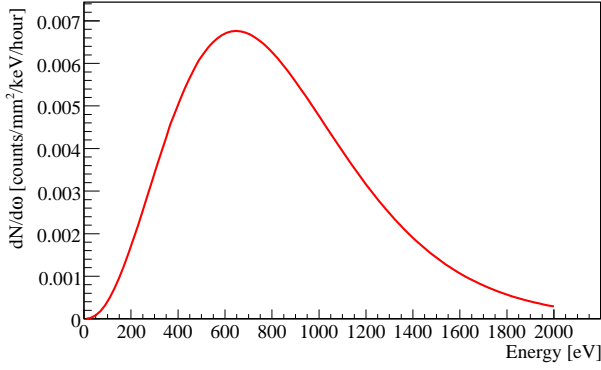


Figure 8: Expected number of photons arriving at the SDD, for $\beta_\gamma^{\text{sun}} = 10^{10.81}$, assuming all chameleons pass through the full magnetic length of the CAST magnet and assuming no absorbing material upstream of the cold bore.

were that 15.7% of emitted chameleons passed through the full field length, the remainder pass through varying lengths (L) which when integrated and scaled by the $(L/L_0)^2$ factor are equivalent to a further 23.2% passing through the full length. In total a scale factor (F) of 38.9% has to be applied to the expected number of photons to account for the fact that not all chameleons that reach the detector pass through the full magnetic length.

All chameleons from the tachocline incident on the SDD must pass via the lead shielding on the sunset side of the magnet before entering the magnet cold bores. The 400 eV energy threshold in the analysis is well above the maximum chameleon effective mass in lead ($m_{\text{eff}}=135$ eV for $n=1$, $\beta_m = 10^6$), hence no absorption effects occur within our region of interest.

The expected number of photons from chameleon conversion inside the CAST magnet, that will reach the SDD is calculated from the theoretical photon spectrum (Fig. 8) arriving at our detector taking into account the total tracking time, the quantum efficiency of the detector, the magnetic length that the chameleons travel inside CAST, the absorption phenomena on the surface of the SDD and the area of the detector:

$$N_i^{\text{ch}} = f(E_i, \beta_\gamma^4) \times A_{\text{SDD}} \times t \times F \times \varepsilon_q \times \varepsilon_{\text{abs}} \times dE, \quad (10)$$

where the index i runs over the energy bins, $f(E_i)$ is the expected number of photons given in $\text{cts}/100 \text{ eV}/\text{mm}^2/\text{s}$ in front of our detector, calculated with $\beta_\gamma^{\text{sun}} = 10^{10.81}$ and having travelled the full length of the CAST magnet, A_{SDD} the area of the detector, t the total tracking time in seconds, ε_q the quantum efficiency of the detector, ε_{abs} the transmission of the thin absorbing layer, that has accumulated after 2 h on its surface, and dE the energy bin size. The resulting spectrum is shown in Fig. 9.

The analysis of the data has been performed by using the likelihood method. For data that follow a Poisson distribution the likelihood function can be expressed as

$$\log(L) = \sum_i (-\lambda_i + t_i \log(\lambda_i) - \log(t_i!)) , \quad (11)$$

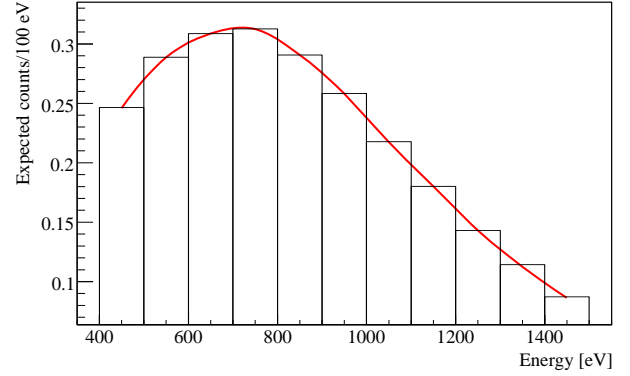


Figure 9: Expected number of photons ($\beta_\gamma^{\text{sun}} = 10^{10.81}$) to be detected by the SDD taking into account the total tracking time.

where t_i is the number of tracking counts in the energy bin i and λ_i is the expected number of counts:

$$\lambda_i = b_i + N_i C, \quad (12)$$

with b_i the expected background in energy bin i and $N_i C$ the expected number of photons from chameleon conversion, which is proportional to the quantity β_γ^4 (eq. 10). For simplicity we choose the free parameter as $C = (\beta_\gamma/\beta_\gamma^{\text{sun}})^4$ to evaluate the data.

The maximum of $\log(L)$ will be achieved by tuning the parameter C . The obtained value $C_{\text{Best fit}}$ is compatible with the null hypothesis within 1 sigma. In Fig. 10 the subtracted counts, tracking minus background (normalised to tracking time), together with the expected photon signal from chameleon conversion, and the best fit to our data are shown.

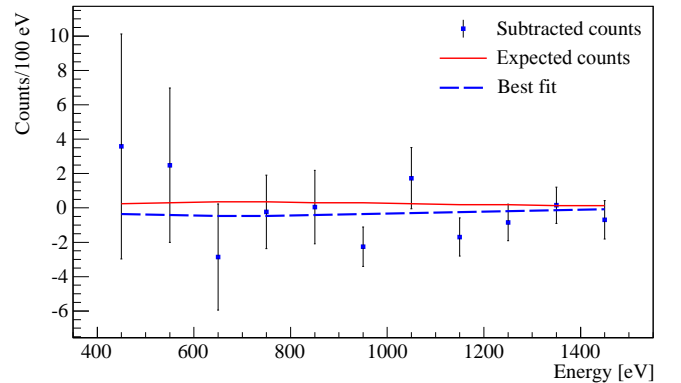


Figure 10: Subtracted counts, expected number of counts during the solar tracking (red) and best fit to the data from the maximisation of the Likelihood (blue).

The upper limit on β_γ is then obtained by integrating the Bayesian probability with respect to C from 0 up to 95%, considering only the non-negative part of the distribution. The resulting bound on β_γ is

$$\beta_\gamma \leq 9.26 \times 10^{10} \text{ at } 95\% \text{ CL}. \quad (13)$$

Our result can be modulated depending on the type of solar model considered. Indeed, we have focused on the $B = 10 \text{ T}$

case in the tachocline. If this hypothesis is relaxed and fields between 1 T and 100 T are considered, the CAST limit on the photon coupling can be shifted by a factor of plus or minus $10^{1/2}$ as can be seen in Fig. 11. The limit obtained with the SDD is lower than the solar luminosity bound for values of tachocline magnetic fields below 4.9 T.

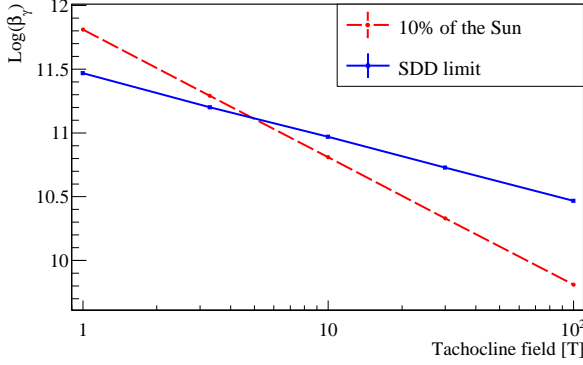


Figure 11: The CAST limit on β_γ for different values of magnetic field in the tachocline.

Additionally, we have shifted the position of the tachocline down to $0.66 R_\odot$ and increased its width from $0.01 R_\odot$ to $0.04 R_\odot$. We have also considered a linearly decreasing magnetic field (10 T at $0.7 R_\odot$ down to 0 T at $0.8 R_\odot$). The changes to the bound on β_γ can be found in Table 1. On the whole and irrespectively of the astrophysics of the tachocline, we have found that the coupling of photons to chameleons satisfies $\beta_\gamma \leq 10^{11}$.

Tachocline [\odot]	Width [\odot]	β_γ at 95% CL	$\beta_\gamma^{\text{sun}}$
0.66	0.04	5.69×10^{10}	2.95×10^{10}
0.66	0.01	8.9×10^{10}	5.89×10^{10}
0.7	0.1 linear	7.29×10^{10}	3.47×10^{10}

Table 1: Upper limit on β_γ derived from our measurements for different solar models, all for 10% solar luminosity bound.

8. Discussion

The parameter space of chameleons is determined by the coupling constants to matter and radiation, and a discrete index n which specifies the type of dark energy model under consideration. Our result for the upper limit on β_γ is presented in Fig. 12, together with other experimental bounds. Some are totally insensitive to the coupling to photons, such as the torsion pendulum tests of the presence of new scalar forces, and therefore result in vertical lines in the figure. Overall, the tests of gravity at the shortest distances lead to a lower bound on the coupling to matter (in green) [21] while test of the modification of the terrestrial gravitational field and its influence on the quantum levels of ultra-cold neutrons lead to an upper bound (lilac) [22] with future experiments in Grenoble by Granit and neutron interferometry promising to lower the limit still further. Presently, the atom-interferometry technique is promising the largest reduction in the upper bound [23]. Precision tests of the standard

model are only sensitive to the coupling to gauge fields, i.e. here to photons, and provide a large upper bound. From astrophysics, an analysis of the polarisation of the light coming from astrophysical objects provides a bound of $\beta_\gamma = 1.9 \times 10^9$ [24].

The results we have presented here for solar chameleons are only valid for values of the matter coupling below the resonance threshold in the production mechanism at the tachocline ($\beta_m < 10^6$). For larger values of the matter coupling, the large values of the mass of the chameleon inside the tachocline compared to the plasma mass lead to a large suppression. The CHASE experiment is sensitive to the photon coupling up to large values of the matter coupling ($\beta_m \sim 10^{14}$). The region above $\beta_m \sim 10^9$ is already excluded by the neutron experiments. At low β_m , our results extend the CHASE coverage by over three orders of magnitude to below $\beta_m = 10$ into a region already excluded by torsion pendulum bounds.

Higher values of n could be envisaged but would not alter the physical picture discussed here (see [7] for a discussion of the $n = 4$ case). Our results are to a large extent insensitive to n (Table 2), provided we are only interested in the region of parameter space below the resonance in the matter coupling.

index n	β_γ at 95% CL
1	9.26×10^{10}
2	9.21×10^{10}
4	9.20×10^{10}
6	9.19×10^{10}

Table 2: Upper limit on β_γ derived at CAST for different values of the index n which defines the chameleon model.

We studied the uncertainties in the assumptions for the solar model and their effect on the CAST result. If for example the solar luminosity bound is reduced by a factor 10, $\beta_\gamma^{\text{sun}}$ is reduced by a factor $10^{1/2}$, whilst β_γ remains constant, resulting in a weaker limit relative to the solar luminosity bound. Rather conservatively, the details of the radial field strength and its distribution at the tachocline may affect the β_γ limit by a factor of 1.6 (Table 1). The largest effect is due to the magnitude of the magnetic field at the tachocline; we have used 10 T and have shown that fields of 1 T or 100 T change β_γ by $10^{1/2}$ up and down respectively (Fig. 11).

All in all, we find that the chameleon parameter space has been significantly reduced. Additional CAST data with the In-Grid detector and an X-ray telescope will improve the photon coupling sensitivity beyond the solar bound in the near future. In parallel CAST is developing a detection technique which exploits the coupling of chameleons to matter. Chameleons of solar origin, focused by an X-ray telescope on CAST, can be directly detected by a radiation pressure device [25].

9. Conclusions

CAST has made a first dedicated sub-keV search for solar chameleons based on the Primakoff effect. This search, running in a vacuum configuration using a readily-available apparatus, did not observe an excess above background and has set a limit

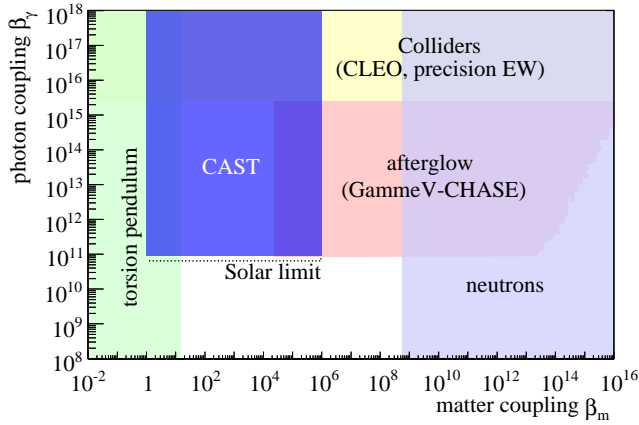


Figure 12: The exclusion region for chameleons in the $\beta_\gamma - \beta_m$ plane, achieved by CAST in 2013 (purple). We also show the bounds set by torsion pendulum tests (in green) [21], resonance spectroscopy measurements of quantum states of ultracold neutrons (lilac) [22], CHASE (pale orange) [11] and collider experiments (yellow) [26].

for the coupling strength to photons which for $n \geq 1$ excludes a new region of parameter space covering 3 orders of magnitude in matter coupling and reaches down to the level of photon coupling corresponding to both the 10% solar luminosity bound and also the limit derived by CHASE.

10. Acknowledgments

We thank CERN for hosting the experiment and for the technical support to operate the magnet and the cryogenics. We thank CERN PH-DT and TE-CRG groups for technical support to build the X-ray detector system and A. Niculae (PNDetector) for technical advice.

We acknowledge support from NSERC (Canada), MSES (Croatia), CEA (France), BMBF (Germany) under the grant numbers 05 CC2EEA/9 and 05CC1RD1/0 and DFG (Germany) under grant numbers HO 1400/7-1 and EXC-153, GSRT (Greece), NSRF: Heracleitus II, RFFR (Russia), the Spanish Ministry of Economy and Competitiveness (MINECO) under Grants No. FPA2008-03456, No. FPA2011-24058 and EIC-CERN-2011-0006. This work was partially funded by the European Regional Development Fund (ERDF/FEDER), the European Research Council (ERC) under grant ERC-2009-StG-240054 (T-REX), Turkish Atomic Energy Authority (TAEK), NASA under the grant number NAG5-10842. Part of this work was performed under the auspices of the U.S. Department of Energy by Lawrence Livermore National Laboratory under Contract No. DE-AC52-07NA27344. P. Brax acknowledges partial support from the European Union FP7 ITN INVISIBLES (Marie Curie Actions, PITN- GA-2011- 289442) and from the Agence Nationale de la Recherche under contract ANR 2010 BLANC 0413 01.

References

[1] E. J. Copeland, M. Sami, S. Tsujikawa, Dynamics of dark energy, *Int. J. Mod. Phys. D* 15 (2006) 1753. [arXiv:hep-th/0603057](#).

[2] T. Clifton, P. G. Ferreira, A. Padilla, C. Skordis, Modified gravity and cosmology, *Phys. Rept.* 513 (2012) 1. [arXiv:1106.2476](#).

[3] J. Khoury, A. Weltman, Chameleon fields: Awaiting surprises for tests of gravity in space, *Phys. Rev. Lett.* 93 (2004) 171104. [arXiv:astro-ph/0309300](#).

[4] J. Khoury, A. Weltman, Chameleon cosmology, *Phys. Rev. D* 69 (2004) 044026. [arXiv:astro-ph/0309411](#).

[5] P. Brax, C. van de Bruck, A. Davis, J. Khoury, A. Weltman, Detecting dark energy in orbit: The cosmological chameleon, *Phys. Rev. D* 70 (2004) 123518. [arXiv:astro-ph/0408415](#).

[6] A. Joyce, B. Jain, J. Khoury, M. Trodden, Beyond the cosmological Standard Model. [arXiv:1407.0059](#).

[7] P. Brax, K. Zioutas, Solar chameleons, *Phys. Rev. D* 82 (2010) 043007. [arXiv:1004.1846](#).

[8] P. Brax, A. Lindner, K. Zioutas, Detection prospects for solar and terrestrial chameleons, *Phys. Rev. D* 85 (2012) 043014. [arXiv:1110.2583](#).

[9] K. Zioutas *et al.*, A decommissioned LHC model magnet as an axion telescope, *Nucl. Instr. and Meth. A* 425 (1999) 480. [arXiv:astro-ph/9801176](#).

[10] P. Brax, A. Upadhye, Chameleon fragmentation. , *JCAP* 1402 (2014) 018. [arXiv:1312.2747](#).

[11] J. H. Steffen *et al.*, Laboratory constraints on chameleon dark energy and power-law fields, *Phys. Rev. Lett.* 105 (2010) 261803. [arXiv:1010.0988](#).

[12] A. Upadhye, J. H. Steffen, A. S. Chou, Designing dark energy afterglow experiments, *Phys. Rev. D* 86 (2012) 035006. [arXiv:1204.5476](#).

[13] K. Zioutas *et al.* (CAST Collaboration), First results from the CERN Axion Solar Telescope (CAST), *Phys. Rev. Lett.* 94 (2005) 121301. [arXiv:hep-ex/0411033](#).

[14] S. Andriamonje *et al.* (CAST Collaboration), An improved limit on the axion-photon coupling from the CAST experiment, *JCAP* 0704 (2007) 010. [arXiv:hep-ex/0702006](#).

[15] E. Arik *et al.* (CAST Collaboration), Probing eV-scale axions with CAST, *JCAP* 0902 (2009) 008. [arXiv:0810.4482](#).

[16] M. Arik *et al.* (CAST Collaboration), Search for sub-eV mass solar axions by the CERN Axion Solar Telescope with ^3He buffer gas, *Phys. Rev. Lett.* 107 (2011) 261302. [arXiv:1106.3919](#).

[17] M. Arik *et al.* (CAST Collaboration), Search for solar axions by the CERN Axion Solar Telescope with ^3He buffer gas: Closing the hot dark matter gap, *Phys. Rev. Lett.* 112 (2014) 091302. [arXiv:1307.1985](#).

[18] C. Krieger, J. Kaminski, K. Desch, InGrid-based X-ray detector for low background searches, *Nucl. Instr. and Meth. A* 729 (2013) 905.

[19] E. Gatti, P. Rehak, Semiconductor drift chamber-an application of a novel charge transport scheme, *Nucl. Instr. and Meth. A* 225 (1984) 608.

[20] T. Vafeiadis, Contribution to the search for solar axions in the CAST experiment, PhD thesis. CERN / Aristotle University of Thessaloniki, Thessaloniki (Greece) CERN-THESIS-2012-349.

[21] A. Upadhye, Dark energy fifth forces in torsion pendulum experiments, *Phys. Rev. D* 86 (2012) 102003. [arXiv:1209.0211](#).

[22] T. Jenke *et al.*, Gravity resonance spectroscopy constraints dark energy and dark matter scenarios, *Phys. Rev. Lett.* 112 (2014) 151105. [arXiv:1404.4099](#).

[23] P. Hamilton, M. Jaffe, P. Haslinger, Q. Simmons, H. Müller, Atom-interferometry constraints on dark energy. [arXiv:1502.03888](#).

[24] C. Burrage, A. Davis, D. J. Shaw, Detecting Chameleons: The Astronomical Polarization Produced by Chameleon-like Scalar Fields, *Phys. Rev. D* 79 (2009) 044028. [arXiv:0809.1763](#).

[25] S. Baum, G. Cantatore, D. H. H. Hoffmann, M. Karuza, Y. K. Semertzidis, A. Upadhye, K. Zioutas, Detecting solar chameleons through radiation pressure, *Phys. Lett. B* 739 (2014) 167. [arXiv:1409.3852](#).

[26] P. Brax, C. Burrage, A. Davis, D. Seery, A. Weltman, Collider constraints on interactions of dark energy with the standard model, *JHEP* 0909 (2009) 128. [arXiv:0904.3002](#).